Solar Energy
And Sustainable Development
Refereed, biannual scientific journal issued by:
The Libyan Center for Solar Energy Research and Studies

Design and optimization of plasmonic nanoparticles-enhanced perovskite solar cells using the FDTD method

Mohammed. M. Shabat[1,2], Hala J. El-Khozondar[3,4*], Salah A. Nassar[2], Guillaume Zoppi[1], Yasser F. Nassar[5].

[1]Department of Mathematics, Physics & Electrical Engineering, Northumbria University, Newcastle upon Tyne, NE1 8ST, UK.

[2]Departement of Physics, Islamic University of Gaza, P.O. Box 108, Gaza Strip, Palestine.

[3]Electrical Engineering and Smart Systems Departments, Islamic University of Gaza, P.O.Box 108, Gaza, Palestine.

[4]Department of Materials and London Centre for Nanotechnology, Imperial College London, UK.

[5]Mechchanical Eng. Dept., Eng. Faculty, Islamic Univ. of Gaza, Gaza Strip, Palestine.

E-*mail:* mohammed.shabat@northumbria.ac.uk , h.elkhozondar@ic.ac.uk , yasser_nassar68@ymail.com.

ARTICALE INFO.

Article history:
Received 25 Jan 2024
Received in revised form 26 Jan 2024
Accepted 8 Mar 2024
Available online 13 Mar 2024

KEYWORDS

nanoparticle, perovskite, solar cell, plasmon, FDTD.

ABSTRACT

This study explores how plasmonic nanoparticles affect absorption, transmission, and reflection—three important performance metrics in organic-inorganic halide perovskite solar cells (PSCs). Through an investigation of different types of nanoparticles and their concentration in the composite layer, the study provides important information for improving PSC design in order to increase overall efficiency. The results highlight the importance of the type and volume fraction of nanoparticles in the composite layer, which influence the spectral characteristics of the solar cell, such as absorption, reflection, and transmission.

These findings could encourage PSCs to be widely used as a practical and affordable renewable energy source, which would advance the development of affordable and efficient solar energy technologies.

*Corresponding author.

DOI: https://doi.org/10.51646/jsesd.v13i1.170

تصميم وتحسين خلايا البيروفسكايت الشمسية المعززة بالجسيمات النانوية البلازمية باستخدام طريقة النطاق الزمني للفرق المحدود

محمد موسى شبات، هالة جارالله الخزندار، صلاح نصار، جولاومي زوبي، ياسر فتحي نصار.

ملخص: تستكشف هذه الدراسة كيف تؤثر الجسيمات النانوية البلازمونية على الامتصاص والنقل والانعكاس - ثلاثة مقاييس أداء مهمة في الخلايا الشمسية البيروفسكيت العضوية غير العضوية الهاليدية. من خلال التحقيق في الأنواع المختلفة من الجسيمات النانوية وتركيزها في الطبقة المركبة، توفر الدراسة معلومات مهمة لتحسين تصميم الجسيمات النانوية الصلبة من أجل زيادة الكفاءة الإجمالية. وتبرز النتائج أهمية نوع وكسر حجم الجسيمات النانوية في الطبقة المركبة، والتي تؤثر على الخصائص الطيفية للخلية الشمسية، مثل الامتصاص، والانعكاس، والنقل. ويمكن أن تشجع هذه النتائج الشركات الخاصة على الاستخدام على نطاق واسع كمصدر عملي وميسور للطاقة المتجددة، مما من شأنه أن يدفع قدما بتطوير تكنولوجيات للطاقة الشمسية تتسم بالكفاءة وبأسعار معقولة.

1. INTRODUCTION

1.1. Background

Among renewable energy sources, solar energy has become a leading contender. Solar energy uses photovoltaics (PV) or solar cells to capture solar radiation and convert it into clean, sustainable electrical energy.

Because solar energy is affordable, environmentally friendly, and able to meet the growing demand for energy worldwide, it has drawn a lot of attention as a possible replacement for conventional fossil fuels. The installed capacity of photovoltaic solar energy has been rising steadily since 2000, and a peak of 1177 GW is anticipated in 2022. Global markets are significantly shifting toward renewable and sustainable energy sources as a result of this expanding trend in the photovoltaic solar energy sector. The photovoltaic solar energy industry has seen significant growth, with the United States and China emerging as leaders with installed capacities of 122 GW and 307 GW, respectively. Moreover, in terms of their total energy mix in 2022, Chile and Honduras claimed the highest percentages of photovoltaic solar energy [1, 2].

PV solar energy fields are extremely important, especially considering how well they work in hybrid energy systems as an ideal complement to conventional and renewable energy sources. Due to their robustness and dependability in producing energy from a variety of sources, such as PV/grid, PV/wind, PV/diesel, PV/concentrated solar power (CSP), PV/wind/diesel, and PV/wind/battery configurations, hybrid energy systems are widely used throughout the world [3-7]. PV Solar systems are employed in a variety of applications because to their versatility, convenience of use, and quick and inexpensive installation. They can have a broad variety of capacity, from milliwatts to many gigawatts, as seen in strategic photovoltaic solar fields [8-12].

In addition to leveraging solar cell fields to maintain and stabilize the network and reduce power fluctuations [13].

The efficiency of solar cells, which determines their ability to convert sunlight into electricity, relies on several factors, including the choice of materials utilized in their fabrication [14-19]. Among the various materials explored, silicon stands out as a preferred option due to its exceptional stability, non-toxicity, well-established manufacturing processes, and abundant availability in the Earth's crust. Consequently, silicon-based solar cells dominate the market, constituting a substantial portion of the photovoltaic industry [20].

Recent advancements in the field have spurred an increased interest in exploring the impact of metal nanoparticles on enhancing solar cell efficiency [21]. Metal nanoparticles, such as Silver (Ag), Gold (Au), and Aluminum (Al), exhibit unique properties, including localized surface plasmons, which make them particularly alluring for enhancing solar cell performance [22].

Localized surface plasmons in metal nanoparticles can lead to a phenomenon known as enhanced light trapping, whereby the path length of light within the solar cell is effectively increased, resulting in greater absorption of sunlight and improved energy conversion [23].
Researchers have delved into diverse solar cell structures and designs aimed at minimizing light reflection and maximizing overall efficiency. The incorporation of single silicon interlayer nanoparticles has emerged as a promising approach to enhance solar cell efficiency further [24]. Additionally, plasmonic thin solar cell structures containing metal nanoparticles have demonstrated their potential in reducing light reflection, thus increasing light absorption and consequently boosting energy conversion efficiency [24].
The field of photovoltaics could undergo a revolution if the impact of metal nanoparticles on solar cell efficiency is further investigated. Scientists and engineers are working to maximize the performance of solar cells through ongoing research and development, making solar energy an even more appealing and practical option for supplying our energy needs in a sustainable and environmentally responsible way [25, 26].
Advanced numerical techniques are needed to analyze and optimize solar cell structures to reduce reflection while maximizing absorption and transmission. Finite Difference Time Domain and the Transfer Matrix Method have both been successful in modelling such intricate structures [27]. The goal of this study is to use the Finite Difference Time Domain method to evaluate the effect of nanoparticles on the absorption spectra inside a hypothetical solar cell structure.
Methylammonium lead halide (MAPbI3) or (CH3NH3 PbI3) perovskite-based solar cells (PSCs) have gained considerable attention due to their outstanding performance characteristics. These solar cells are renowned for their high efficiency, cost-effectiveness, flexibility, transparency, and direct-band gap property. Despite these advantages, there are still challenges to address. One significant concern is the toxicity of lead in MAPbI3 PSCs, with thicker perovskite films posing a higher risk [28]. To address this problem, scientists are investigating ways to reduce toxicity while maintaining solar absorption and cell performance by optimizing film thickness to below 350 nm. The limited infrared absorption of MAPbI3 PSCs presents another difficulty. To expand the absorption range into the infrared region, researchers are actively working on solutions like incorporating new materials or changing the composition of perovskite films. The potential for MAPbI3 PSCs to completely change the solar energy sector will increase by addressing these performance issues [29].

1.2. Motivation

The biggest problem facing researchers in this field is producing high-performing solar cells with the least amount of environmental toxicity possible. This encourages the authors to suggest a solar cell that satisfies environmental standards while improving performance.
Furthermore, writers are employed in nations located in the hot zone. This indicates that these nations are interested in creating a new industrial area for the production of solar cells, which makes the study beneficial to the community.

1.3. Aims

The aim of the study is to present a modified solar cell. The proposed solar cell consists of both nanomaterials and Perovskite structure solar cells. Metal nanostructures have a special localized plasmonic effect that can be used to increase light-trapping effectiveness at longer wavelengths. The localized surface plasmon resonance (LSPR) in metallic nanoparticles lengthens the time that light and matter interact, increasing the amount of light that can be absorbed by the thin perovskite films used in solar cells. Furthermore, a higher absorption efficiency within PSCs can be attained by utilizing the far-field scattering effect of surface plasmons.

2. DEVICE STRUCTURE

The basic optical diagram of the solar cells under consideration is shown in Fig. 1. In order to increase the effectiveness of the suggested solar cells, the optical model incorporates nanoparticles (NPs), which produce localized surface plasmons through interaction with light. The plasmonic thin film solar cell's unit cell, which has a four-layered structure, is shown in the illustration. Metal nanoparticles (Ag, Al, or Au) are present in the top layer, which is followed by indium tin oxide (ITO), a perovskite active layer ($CH_3NH_3PbI_3$) acting as the absorbent material, and finally a ZnS substrate. These layers' individual thicknesses are designated as d_0, d_1, d_2, and d_3, respectively.

The structure's periodicity is denoted by the letter P, and the p-polarized incident light enters the structure through the metal nanoparticles. The device's geometrical parameters are d_0=25 nm, d_1=25 nm, d_2=120 nm, d_3=40 nm, and P=200 nm. The solar cell structure's materials are based on information from [30]. Additionally, the perovskite-based solar cells' (PSC) complex refractive index is defined as n+ik, where n is equal to 2.4293 and k is equal to 0.38085[31].

A Perfectly Matched Layer (PML) is used as a boundary in the structure to stop reflections and absorb all emitted electromagnetic waves. It gradually rises from zero to a maximum value at the front interface of the PML as the conductivity (y) within the PML is smoothly graded. [30] provides a description of the conductivity polynomial grading. For simulating the behavior of electromagnetic waves, the Finite Difference Time Domain (FDTD) method is a common computational approach. A PML encircles the computational domain, absorbing the incident waves, to prevent the reflection of scattered waves from the boundaries. To avoid reflections, the impedance of the computational domain and the PML must be perfectly matched [31].

At the front interface of the PML, a polynomial grading of conductivity with a smooth transition from zero to maximum conductivity is implemented [30]. The behavior of conduction electrons inside a metal is taken into account by the Lorentz-Drude model, which is widely used to describe the permittivity of metals [32].

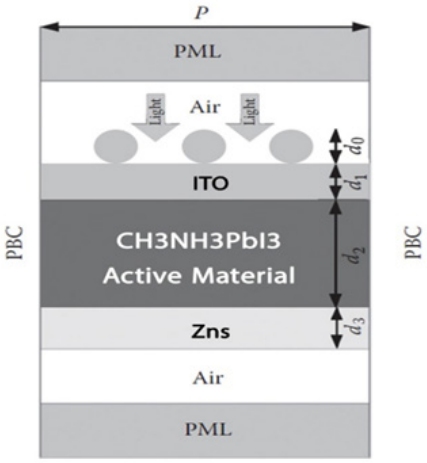

Fig. 1: Schematic Diagram of Plasmonic Solar Cell with Metal Nanoparticles.

3. METHODOLOGY

Our study's notation and methodology are in line with earlier studies [33]. When a broadband analysis is required in numerical electromagnetics, such as in solar cells, finite-difference time-domain (FDTD) is a helpful technique. The central difference approximation is used by the FDTD method to discretize the Maxwell equations in both the time and spatial domains. The Finite Difference Time Domain (FDTD) method, which involves defining a finite computation

domain and putting in place absorbing boundary conditions, is the computational strategy used in our study. In the FDTD method, an incident wave interacts with an object and scatters in various directions and at various rates. A Perfectly Matched Layer (PML) is used to make sure that scattered waves do not result in reflections at the edges of the computation domain. In order to effectively absorb the incident waves and prevent reflections, the PML is made to have an impedance that precisely matches the computation domain [30]. One benefit of the FDTD method over the finite element method (FEM) is the PML, which allows for more appropriate simulation of problems with unclosed spaces. [34].

We use the periodic boundary condition (PBC) in our application of the FDTD method. Using this method, the field values at one edge of the simulation region are duplicated and then introduced at the opposite edge. We can simulate periodic structures and keep the fields continuous across all boundaries in the computational domain by using the PBC. Equations 1 and 2's FDTD numerical solutions came about as a result of discretizing integral forms of Maxwell's equations [30].

$$\frac{1}{\Delta t}\int_A (B^{n+1/2} - B^{n-1/2}).nds = -\int_{\partial A} (E^n).dl \qquad .....(1)$$

$$\frac{1}{\Delta t}\int_A (D^{n+1/2} - D^n).nds = -\int_{\partial A^*} (H^{n+1/2}).dl \qquad .....(2)$$

Where the magnetic and electric fields *E, D, B*, and *H* are in vector form. The line integral on the right side of (1) represents the electric circulation around the curve ∂A, which is an electric contour. The line integral on the right side of equation (2) stands in for the magnetic circulation around curve ∂A^*, which is a magnetic contour. The superscript indicates the time scale at which the variables are evaluated. The airborne composite layer of nanoparticles' effective refractive index (ε_{eff}) is defined as follows:

$$\varepsilon_{eff} = \varepsilon_h \frac{\varepsilon_i(1+2f) + 2\varepsilon_h(1-f)}{\varepsilon_i(1-f) + \varepsilon_h(2+f)} \qquad .....(3)$$

Where *f* is the volume fraction of the particle in the host medium and ε_h is the permittivity of the host (in this case, air), ε_i is the permittivity of the nanoparticle's materials. The nanoparticle's volume fraction (*f*) can be expressed as [35].

$$f = \frac{(N_p \times V_p)}{V_{layer}} \qquad .....(4)$$

where $V_{layer}=Lld$ and $l=d$ are the nanoparticle's radii and *L* is the length of the solar cell surface. The spherical particle's volume (*Vp*) is equal to $4\pi d^3/3$. p is the period of the two-dimensional array, and *(L/p)x(l/p)* is the number of particles on the surface (*Np*).

Assuming that sunlight consists of both TE and TM spectra, the calculation is done for both of them. Thus, the powers of absorption, transmission, and reflection are determined for both spectra. After that, the sum of the TE and TM absorption, transmission, and reflection spectra is used to calculate the total absorption, transmission, and reflection spectra. We only took normal incidence into consideration in this study. Both TE and TM are equal in this situation. Therefore, all that is needed to obtain the desired absorption spectrum is to study one of them.

4. RESULTS AND DISCUSSION

The numerical analysis is done using the Maple program. In the analysis, Three NP materials are considered which are: Silver (Ag), Gold (Au), and Aluminium (Al). The absorption spectra of the proposed solar cell structure for different NP volume fractions (*f*) are shown in Figs. 2-4 for each material. In all cases, f is chosen to have the following values: 0.1, 0.2, 0.3, and 0.4. Fig. 2 shows the absorption spectra for the proposed solar cell using different silver (Ag) nanoparticle fraction *f*.

It can be easily seen from Fig. 2 that as silver fraction increases the absorption spectrum increases around 350 nm, 450 nm, and 620 nm. It is also noticeable that peaks for the spectrum at different volume fractions correspond to different values of wavelength referring to the shift induced by the nanoparticle. Fig. 3 displays the absorption spectrum for the proposed solar cell at different values of gold nanoparticle (Au) fraction *f*. The figure shows that absorption increases as the increase of *f*. It reaches its maximum values around 320 nm, 480 nm, and 680 nm. No wavelength shift is noticed in this case at different values of gold nanoparticle (Au) fraction *f*.

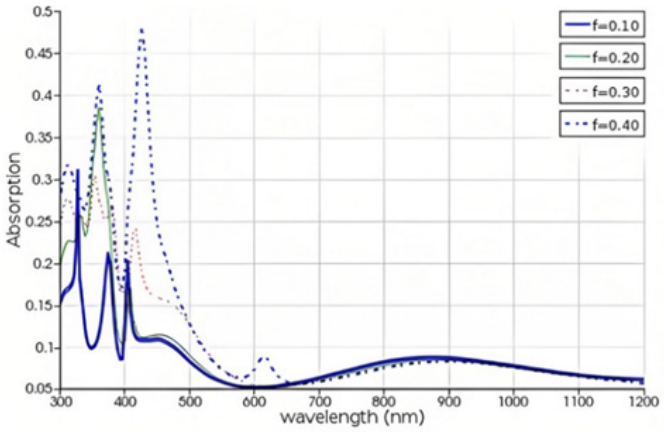

Fig. 2: Absorption spectra with silver (Ag) nanoparticles in front layer with different values of *f* .

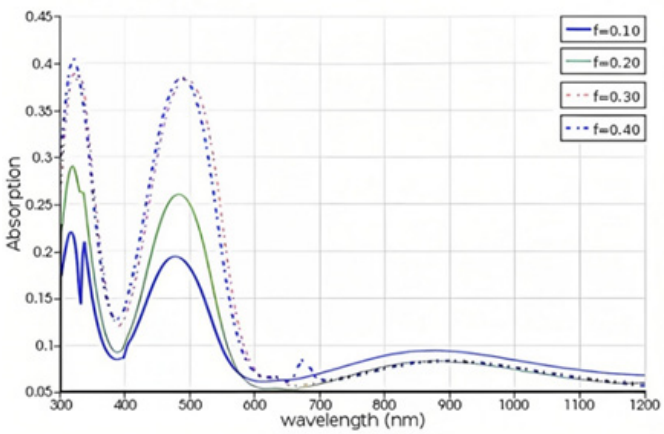

Fig. 3: The absorption spectra in the proposed solar cell structure for different values of the volume nanoparticles fractions of gold metals (Au).

The same calculations for absorption spectrum are repeated for Aluminium nanoparticle (Al) as shown in Fig. 4. In Fig. 4, it can be seen that the absorption increases with increasing the fraction of Al in the structure. It is represented in the peaks around 320-380 nm, around 420-480nm, and around 860-920 nm. It is also noticeable that there is a small shift between the peaks for the spectrum at different volume fractions. The calculations for the transmission spectra for different nanoparticles at different volume fractions are displayed in Figs. 5 and Fig.7. At different values of volume fraction of silver (Ag), the transmission spectrum is plotted in Fig. 5. The spectrum decreases as increasing *f* in the range of wavelength between 300-450nm. Afterward, we see an increase in the transmission spectrum with increasing *f* till around 620 nm. Afterward, the spectrum decreases with increasing *f* till 900 nm and then increases again with increasing the value of *f*. It may also be realizable that the peaks for each spectrum have a small shift compared to each other.

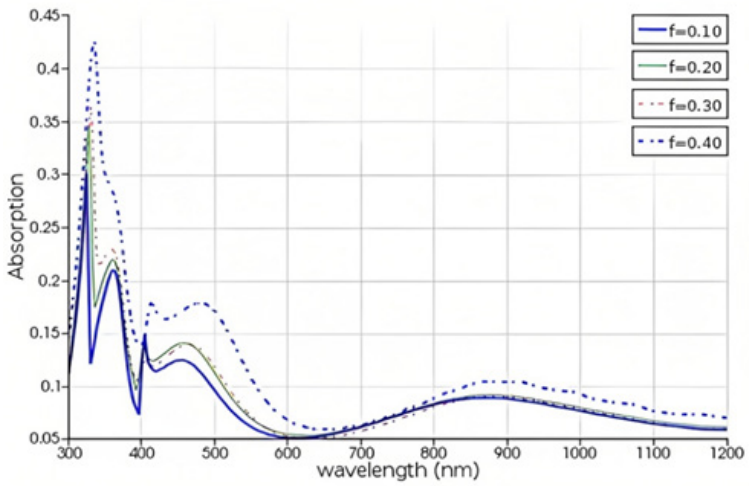

Fig. 4: The absorption spectra in the proposed solar cell structure for different values of the volume nanoparticles fractions (f) of Aluminium metals (Al).

The transmission spectrum for solar cells is displayed in Fig. 6 at different values of volume fraction (f) of gold nanoparticles (Au).
We realize again that as f of the gold nanoparticle increases the spectrum decreases till 550 nm then it increases with increases f till wavelength 650 nm and increases again with f after 900 nm with the small shift between peaks that corresponds to different values of f.
Changing the nanoparticle to Al, The transmission spectrum for solar cells is displayed in Fig. 7 at different values of volume fraction (f) of Al.
It is shown in the figure the spectrum decreases as f of the Al nanoparticle increases except for the range between 520-620 nm and above 920 nm. It is also displayed that there are shifts between the peaks of each spectrum due to the different values of f. where the peaks of the spectrum with higher values of f shift to higher wavelengths.

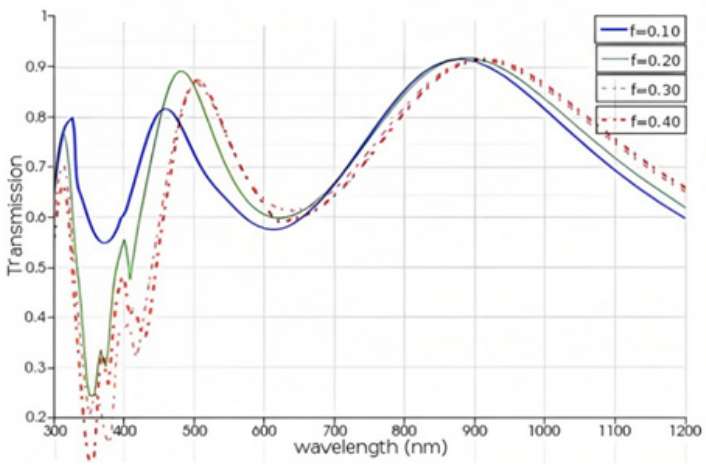

Fig. 5: Transmission spectrum for the proposed solar cell at different values of f for silver (Ag) nanoparticles in the front layer.

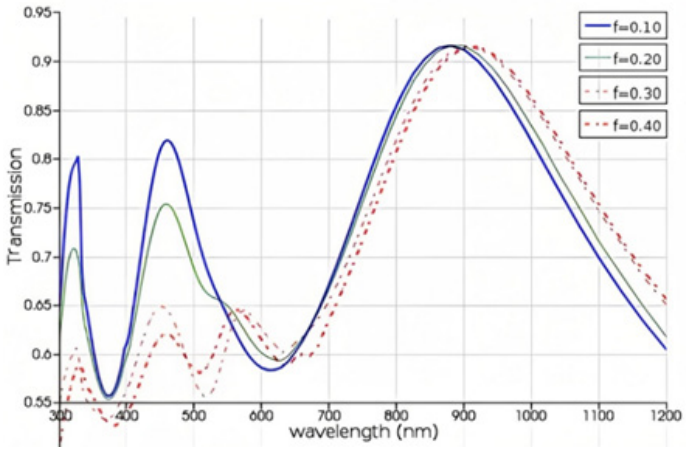

Fig. 6: Transmission spectra for the proposed solar cell at different fractions *f* for gold (Au) nanoparticles in the front layer.

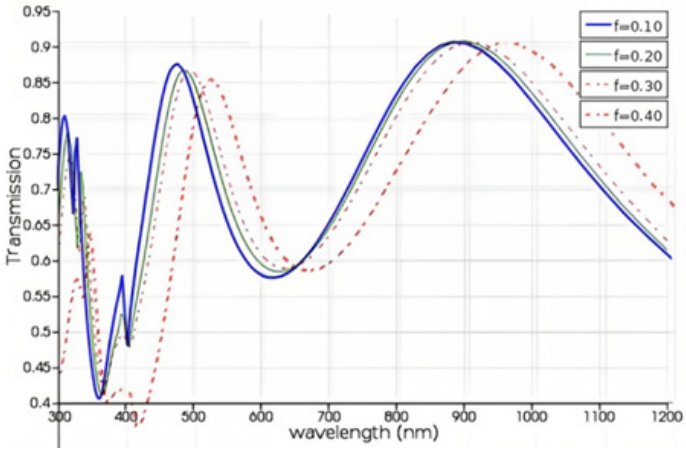

Fig. 7: Transmission spectrum for the solar cell at different values of volume fraction (*f*) of Aluminium (Al) nanoparticles in the front layer.

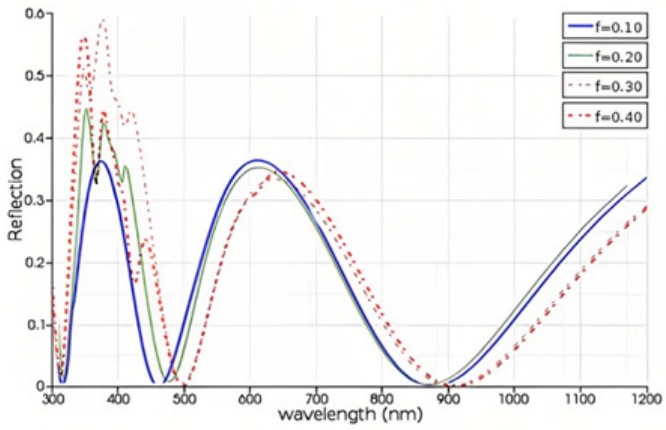

Fig. 8: Reflection spectra at different volume fractions of silver (Ag) nanoparticles in the front layer.

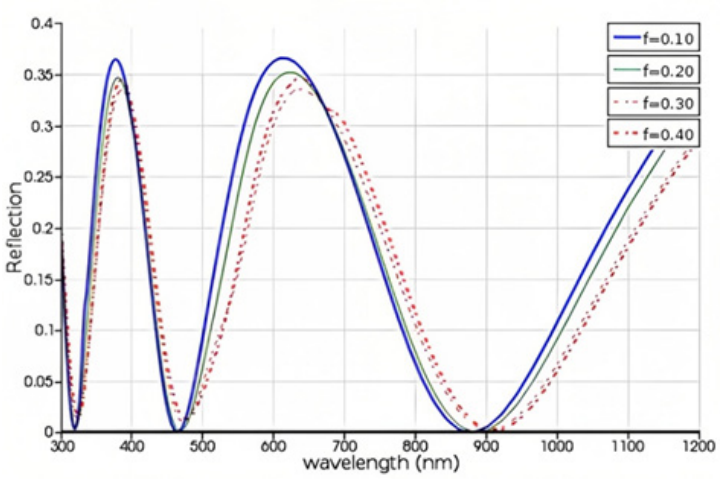

Fig. 9: Reflection spectra at different values of volume faction of gold (Au) nanoparticles in the front layer.

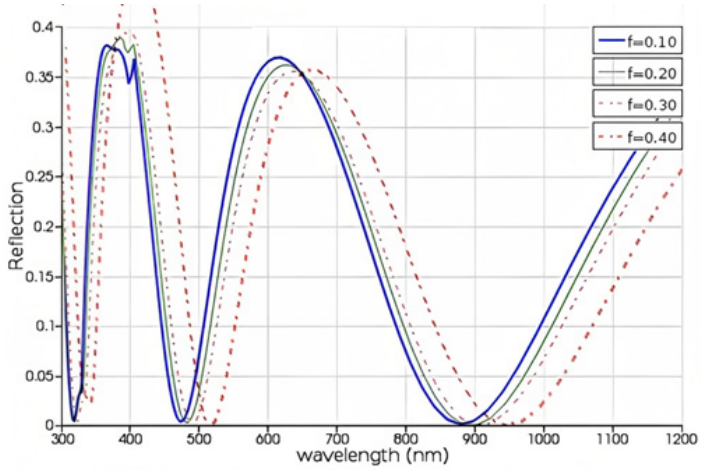

Fig. 10: Reflection spectra at different values of volume fraction of aluminium (Al) nanoparticles in the front layer.

The reflection spectrum for the proposed solar cell is presented in Figs. 8-10 for different values of volumes fractions of different nanoparticles (Ag, Au, and Al).

Fig. 8 displays the reflection spectrum of the proposed solar cells as changing the value of *f* for Ag nanoparticle. It is noticeable that the reflection increases with increasing the value of *f* for Ag nanoparticles except at wavelength 500-650nm and above 900nm. In addition, it is also clear that there is a shift in the spectrum at different values of *f*.

The reflection spectrum for the solar cell at different values of *f* for Au nanoparticle in Fig. 9 shows that as *f* increases the reflection decreases except at the wavelength ranges from 420 -500 nm and from 680-900 nm where the reflection spectrum increases with increasing the value of *f*. It also displays a shift in the spectrum to higher wavelengths as *f* value increases. Similarly, the reflection spectrum for a solar cell with Al nanoparticles at different values of *f* is shown in Fig. 10. The reflection increases as f increases for wavelengths ranging from 380-580 nm and 650-920 nm. Also, the reflection spectrum shifts to a higher wavelength as *f* values increase.

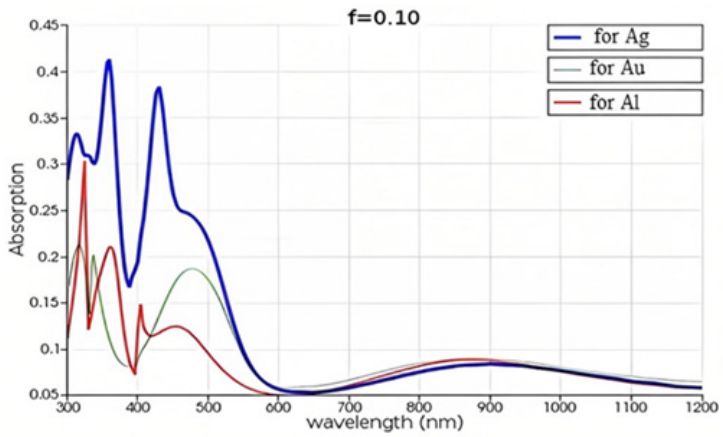

Fig. 11: Absorption spectra depicting three distinct types of nanoparticles at a volume fraction (f) of 0.1.

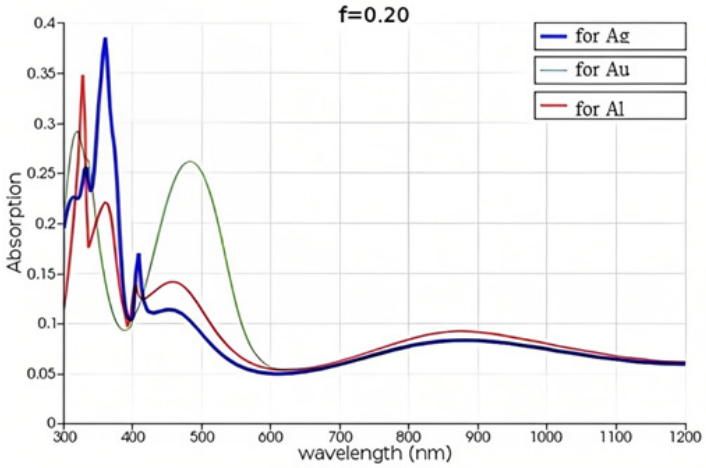

Fig. 12: Absorption spectra depicting three distinct types of nanoparticles at a volume fraction (f) of 0.2.

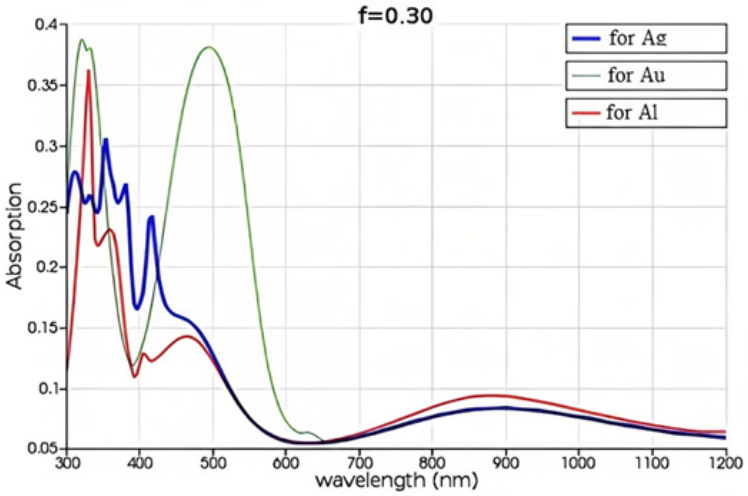

Fig. 13: Absorption spectra depicting three distinct types of nanoparticles at a volume fraction (f) of 0.3.

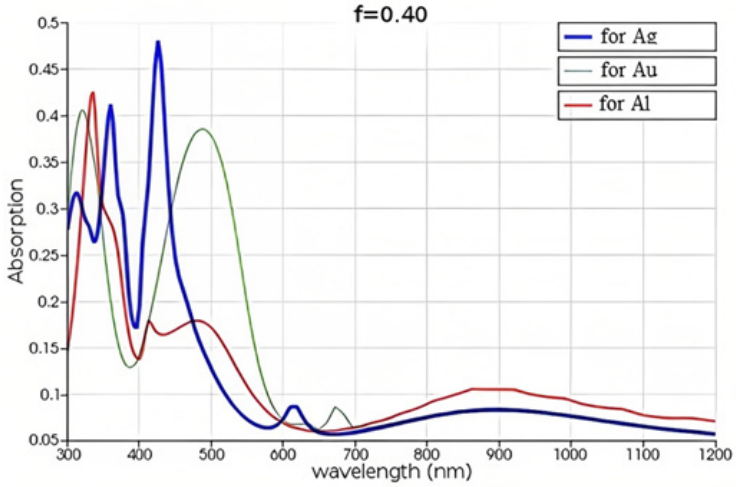

Fig. 14: Absorption spectra depicting three distinct types of nanoparticles at a volume fraction (f) of 0.4.

Figs 11-14 display the absorption spectrum for the proposed solar cell for different nanoparticles at different volume fractions of the. Fig. 11 shows the absorption spectra for Ag, Au, and Al at volume fraction f = 0.1. The absorption spectra have the highest values for a solar cell with Ag nanoparticles in the front layer for wavelength ranges from 300-600 nm afterward the highest values correspond to a solar cell with Au nanoparticles in the front layer. The absorption spectra at different nanoparticles for f = 0.2 are shown in Fig. 12. In this case, the spectrum varies with the type of nanoparticle such that it increases and decreases for different nanoparticles at different wavelengths. For example, at 320 nm the highest spectrum occurs for Al nanoparticles while at 450 nm is for Ag nanoparticles, and between 420-600nm the increase corresponds to the spectrum with Au nanoparticles. Similar behavior of the spectrum at volume fractions 0.3 and 0.4 in Figs. 13 and 14 can be seen.

5. CONCLUSION

A suggested solar cell featuring a perovskite absorption layer covered with composite layer of nanoparticles. The structure is used to reach high-performance solar cells. In addition, PML layer is used to absorb the scattered waves and prevent reflections, while the polynomial grading of conductivity within the PML ensures a smooth transition. The FDTD method is used to simulate the behaviour of electromagnetic waves. The Lorentz-Drude model is used to describe the permittivity of metals, and the periodic boundary condition is used to copy fields in the simulation region. The values of the volume fraction of nanoparticles f and the type of nanoparticles are used to verify the effect of nanoparticles on the behaviour of the solar cell. In the calculations, Ag, Au, and Al are used in the nanocomposite. The results show that the spectrum of the solar cell is affected by both the type of nanoparticle and its volume fraction f. It is possible to extend the study to include other nanoparticles, such as Cu. Additionally, the computation may investigate how each layer's thickness and particle size affect the performance of the cell.

Author Contributions: All authors have made a substantial, direct, and intellectual contribution to the work and approved it for publication.
Funding: This research received no external funding.
Data Availability Statement: Data will be available upon request.
Conflicts of Interest: The authors declare that they have no conflict of interest.

REFERENCES

[1] Y. F. Nassar, El-Khozondar, H. J., Alatrash, A., Ahmed, B., Elzer, R., Ahmed, A., Imbayah, I., Alsharif, A., Khaleel, M., "Assessing the viability of solar and wind energy technologies in semi-arid and arid regions: a case study of Libya's climatic conditions," Applied solar energy, vol. 60, no. 1, p. under press, 2024.

[2] A. H. Alsharif, Ahmed, A. A., Nassar, Y. F., Khaleel, M. M., El-Khozondar, H. J., Alhoudier, T. E., Esmail, E. M. , "Mitigation of dust impact on solar photovoltaics performance considering Libyan climate zone: a review," Wadi Alshatti Univeristy Journal of pure and applied sciences, vol. 1, no. 1, pp. 22-27, 2023.

[3] Y. F. Nassar, Abdunnabi, M. J., Sbeta, M. N., Hafez, A. A., Amer, K. A., Ahmed, A. Y., Belgasim, B., "Dynamic analysis and sizing optimization of a pumped hydroelectric storage-integrated hybrid PV/Wind system: A case study," Energy Conversion and Management, vol. 229, p. 113744, 2021.

[4] H. J. El-Khozondar, El-batta, F., EL-Khozondar, R. J., Nassar, Y., Alramlawi, M., Alsadi, S., "Standalone hybrid PV/wind/diesel-electric generator system for a COVID-19 quarantine center," Environmental Progress & Sustainable Energy, vol. 2, no. 3, p. e14049, 2023.

[5] Y. F. Nassar, Alsadi, S. Y., El-Khozondar, H. J., Ismail, M. S., Al-Maghalseh, M., Khatib, T., Sa'ed, J. A., Mushtaha, M. H., Djerafi, T., "Design of an Isolated Renewable Hybrid Energy System: A Case Study," Materials for Renewable and Sustainable Energy, vol. 11, no. 3, pp. 225-240., 2022.

[6] M. Almihat, Kahn, M., "Design and implementation of Hybrid Renewable energy (PV/Wind/Diesel/Battery) Microgrids for rural areas," Solar Energy and Sustainable Development Journal, vol. 12, no. 1, pp. 71–95, 2023.

[7] L. Rtemi, El-Osta, W., Attaiep, A., "Hybrid System Modelling for Renewable Energy Sources," Solar Energy and Sustainable Development Journal, vol. 12, no. 1, pp. 13–28, 2023.

[8] A. K. H. Elfaqih, "Design of photovoltaic system powered a small-scale SWRO desalination plant," Solar Energy and Sustainable Development Journal, vol. 5, no. 1, pp. 12-21, 06/30 2016.

[9] G. Azzain, Lali, I., "An Economical -Technical Comparison of Solar Electrical Water Pumping System Versus Conventional Electrical Water Pumping System for Agricultural Purposes in the Area of "Awjila"," Solar Energy and Sustainable Development Journal, vol. 5, no. 1, pp. 30–43, 2016.

[10] M. Sbeta, Sasi, S., "On the Field Performance of PV Water Pumping System in Libya," Solar Energy and Sustainable Development Journal, vol. 1, no. 1, pp. 1–7, 2012.

[11] K. Alshoshan, El-Osta, W., Kahlifa, Y., Saleh, I., "Feasibility Study of Zero Energy Houses: Case Study of Magrun City - Libya," Solar Energy and Sustainable Development Journal, vol. 7, no. 2, pp. 59–77, 2018.

[12] M. Abdel-Hadi, Aldali, Y., Celik, A., "Validation of Thrmal Models for Polycrystalline Photovoltaic Module Under Derna City Climate Conditions," Solar Energy and Sustainable Development Journal, vol. 7, no. 2, pp. 27–40, 2018.

[13] M. Khaleel, Yusupov, Z., Yasser, N., Elkhozondar, H. J., Ahmed, A., "An Integrated PV Farm to the Unified Power Flow Controller for Electrical Power System Stability," Int. J. Electr. Eng. And Sustain, vol. 1, no. 2, pp. 18–30, 2023.

[14] K. Dadesh, Alarabi, W., "Simulation of a Novel Junction-less Solar Cell Structure Using PC-1D Software," Solar Energy and Sustainable Energy Journal, vol. 10, no. 2, pp. 1–10, 2021.

[15] M. Abdel Hadi, Aldali, Y., Celik, A., "Validation of Thermal Models for Polycrystalline Photovoltaic Module Under Derna City Climate Conditions," Solar Energy and Sustainable Development Journal, vol. 7, no. 2, pp. 27–40, 2018.

[16] R. J. El-khozondar, El-khozondar, H. J., Nassar, Y. F. , "Efficiency performance of Ag-CdSe quantum dots nanocomposite sensitized solar cells," Results in Optics, vol. 13, p. 100516, 2023.

[17] R. J. El-Khozondar, El-khozondar, H. J., Nassar, Y. F., Bayoumi, E. H. E., Awad, H., "Efficiency improvement of Ag-doped CdSe quantum dot sensitized solar cells," presented at the The 8th International Engineering Conference on Renewable Energy & Sustainability (ieCRES 2023), Palestine, 08-09 May, 2023.

[18] S. Elhamali, Akhil, M., Abusabee, K., Kalfagiannis, N., Koutsogeorgis, D. , "Environmental Stability Evaluation of Aluminium Doped Zinc Oxide (AZO) Transparent Electrodes Deposited at Low Temperature for Solar cells," Solar Energy and Sustainable Development Journal, vol. 11, no. 1, pp. 1–12, 2022.

[19] A. Kagilik, "Dry Phosphorus silicate glass etching and surface conditioning and cleaning for multi-crystalline silicon solar cell processing," Solar Energy and Sustainable Development Journal, vol. 3, no. 1, pp. 38–50, 2014.

[20] M. A. Green, Emery, K., Hishikawa, Y., Warta, W., Dunlop, E. D. , "Solar cell efficiency tables (version 54)," Progress in Photovoltaics: Research and Applications, vol. 27, no. 1, pp. 3-12, 2019.

[21] M. F. Ubeid, Shabat, M. M., "Numerical analysis of a multilayer structure containing metal nanoparticles for photonic integrated circuits applications," Romanian Journal of Physics, vol. 66, pp. 1-8, 2021.

[22] H. A. Atwater, Polman, A. , "Plasmonics for improved photovoltaic devices," Nature materials, vol. 9, no. 3, pp. 205-213, 2010.

[23] Y. Zhang, Chen, X., Liu, Y., Yang, D., "Nanoparticle-enhanced light trapping in thin-film silicon solar cells," Nano Energy, vol. 17, pp. 160-175, 2015.

[24] Y. Gao, Chen, Y., Du, B., Ma, R., Zhang, Y., Lu, Z., "Enhanced light absorption in thin-film silicon solar cells with a low-cost and highly efficient back reflector," Optics Express, vol. 24, no. 18, pp. A1288-A1296, 2016.

[25] H. J. El-Khozondar, El-Khozondar, R. J., Shabat ,M., D. Schaadt, D., "Solar cell with multilayer structure based on nanoparticles composite," Optik, vol. 166, pp. 127-131, 2018.

[26] H. J. El-Khozondar, El- Khozondar, Sharma, A., Ahmed, K., Dhasarathan, V. , "Highly efficient solar energy conversion using graded-index metamaterial nanostructured waveguide," Journal of Optical Communications, vol. 1, pp. 1-4, 2020.

[27] H. J. El-Khozondar, Shabat and M. M., AlShembari, A. A., "Characteristics of Si-Solar Cell (PV) Waveguide Structure Using Transfer Matrix Method," presented at the IEEE Promising Electronic Technologies Deir El-Balah, Palestine, 2017.

[28] T. T. Ava, Al Mamun, A., Marsillac, S., Namkoong, G. A . "A Review: Thermal Stability of Methylammonium Lead Halide Based Perovskite Solar Cells," Applied Sciences, vol. 9, no. 1, pp. 188-203, 2019.

[29] S. Bishnoi, Pandey, S. K., "Device performance analysis for lead-free perovskite solar cell optimisation," IET optoelectronics, vol. 12, no. 4, pp. 185-190, 2018.

[30] E. D. Palik, Handbook of Optical Constants of Solids. New York: Harcourt Brace Jovanovich, 1998.

[31] M. S. Alias, Dursun, I., Saidaminov, M. I., Diallo, E. M., Mishra, P., Ng, T. K., Bakr, O. M., Ooi, B. S. , "Optical constants of CH3NH3PbBr3 perovskite thin films measured by spectroscopic ellipsometry," Opt. Express, vol. 24, pp. 16586-16594, 2016.

[32] W. E. I. Sha, Choy, W. C. H., Chew, W. C., "Theoretical Studies of Plasmonic Effects in Organic Solar Cells. In Organic Solar Cells: Materials and Device Physics," in Green Energy and Technology, vol. 128: Springer, 2013, pp. 177-210.

[33] B. Mulyanti, Wulandari, C., Hasanah, L., Pawinanto, R. E., Hamidah, I., "Absorption Performance of Doped TiO2-Based Perovskite Solar Cell using FDTD Simulation," Modelling and Simulation in Engineering, vol. 2022, p. 9299279, 2022/02/27 2022.

[34] G. Haidari, "Towards realistic modeling of plasmonic nanostructures: a comparative study to determine the impact of optical effects on solar cell improvement," Journal of Computational Electronics, vol. 21, pp. 137–152, 2022.

[35] D. M. El-Alamassi, El-Khozondar, H. J., Shabat, M. M., "Efficiency Enhancement of Solar Cell Using Metamaterials," International Journal of Nano Studies & Technology, vol. 4, pp. 84-87, 2015.